

# Variation of Cellulose Microfibril Angles in Softwoods and Hardwoods— A Possible Strategy of Mechanical Optimization

H. Lichtenegger,\* A. Reiterer,† S. E. Stanzl-Tschegg,† and P. Fratzl\*

\**Erich Schmid Institute for Materials Science, Austrian Academy of Sciences and University of Leoben, Leoben, Austria;*  
and †*Institute of Physics and Meteorology and Christian Doppler Laboratory for Fundamentals of Wood Machining,*  
*BOKU Vienna, Austria*

Received July 13, 1999, and in revised form October 5, 1999

**Position-resolved small-angle X-ray scattering** was used to investigate the nanostructure of the wood cell wall in two softwood species (Norwegian spruce and Scots pine) and two hardwood species (pedunculate oak and copper beech). The tilt angle of the cellulose fibrils in the wood cell wall versus the longitudinal cell axis (microfibril angle) was systematically studied over a wide range of annual rings in each tree. The measured angles were correlated with the distance from the pith and the results were compared. The microfibril angle was found to decrease from pith to bark in all four trees, but was generally higher in the softwood than in the hardwood. In Norwegian spruce, the microfibril angles were higher in late wood than in early wood; in Scots pine the opposite was observed. In pedunculate oak and copper beech, low angles were found in the major part of the stem, except for the very first annual rings in pedunculate oak. The results are interpreted in terms of mechanical optimization. An attempt was made to give a quantitative estimation for the mechanical constraints imposed on a tree of given dimensions and to establish a model that could explain the general decrease of microfibril angles from pith to bark. © 1999 Academic Press

**Key Words:** cellulose; hardwood; microfibril angle; small-angle scattering; softwood; wood; X-ray.

## INTRODUCTION

The cellular structure of wood is designed to provide optimum conditions for the tree, using a minimum of material. Softwoods and hardwoods meet these requirements in different ways that result in anatomical differences on the macroscopic scale (e.g., the shape of the trunk) as well as on the microscopic scale (cell morphology). On the micrometer scale, softwoods consist of up to 95% tracheids that fulfill, at the same time, the function of conducting water and sustaining the tree mechanically. In

hardwoods, specialized cells exhibiting different morphologies carry out different tasks (Grosser, 1977). On the nanometer scale, however, the architecture of the wood cell wall essentially follows the same principle: elementary cellulose fibrils with a diameter in the nanometer range embedded in a hemicellulose–lignin matrix are arranged in several layers around the cell (Fengel and Wegener, 1984). In the major part of the cell wall, the S2 layer, the cellulose fibrils run fairly parallel to one another and follow a steep helix around the cell. The angle between the cellulose fibrils and the longitudinal cell axis, the microfibril angle (MFA), was found to be a crucial factor in determining the mechanical properties of wood (Cave, 1989; Cave and Walker, 1994; Reiterer *et al.*, 1999).

The microfibril angle has already been the subject of extensive investigations (see, for example, Jakob *et al.*, 1994; Meylan, 1967; Sahlberg *et al.*, 1997; Wardrop, 1952), most of them concerning softwoods. It has been found that the MFA decreased from pith to bark (e.g., Preston, 1934). There is, however, no consistent explanation for the differences in MFA within a single stem.

In this paper we apply the technology of position-resolved small-angle X-ray scattering (scanning SAXS) (Fratzl *et al.*, 1997) for the systematic determination of the microfibril angle in the S2 layer of the wood cell wall as a function of the distance from the pith. We show that scanning SAXS is an appropriate tool also for the investigation of anatomically different hardwoods. Results from four different wood species are presented: *Picea abies* (Norwegian spruce), *Pinus sylvestris* (Scots pine), *Quercus robur* (pedunculate oak), and *Fagus sylvatica* (copper beech). We compare the variations of the microfibril angle from pith to bark and discuss the differences in view of a mechanical optimization of wood by different microfibril angles.

## MATERIALS AND METHODS

### Sample Preparation

Two softwood species and two hardwood species were selected for the study: *P. abies* (grown in the Erzgebirge, Germany) and *P. sylvestris*, *Q. robur*, and *F. sylvatica* (all three grown in the Wienerwald, Austria). Discs were taken at breast height and one sector was sawed out. Cubes of about  $1 \times 1 \times 1$  cm were cut out along the radius. Radial slices 200  $\mu\text{m}$  thick comprising several annual rings were cut by microtome from all four species and used for small-angle X-ray scattering (SAXS). Additionally, tangential sections of *Q. robur* containing exclusively late wood were prepared. The slices were used as cut, without any further treatment, just encapsulated in plastic foil to keep them from drying and shrinking in the vacuum chamber of the X-ray equipment.

In addition to the samples for the X-ray measurements, wood samples from the same block were dried, washed with alcohol, embedded in methacrylate, and cut to 3- $\mu\text{m}$ -thick cross sections for light microscopy.

### Measurement

A scanning SAXS device (Bruker AXS) was used to determine the microfibril angles in each of the four investigated trees over a wide range of annual rings. The measurements were carried out in point focus geometry using  $\text{CuK}_\alpha$  radiation obtained from a rotating anode generator equipped with Göbel mirrors. The beam width at the sample position was 200  $\mu\text{m}$ . A two-dimensional multiwire detector was used to record the scattering patterns. The distance of the sample to the detector was 63 cm. The sample was placed on a computer-controlled movable stage and could be scanned through the beam in two orthogonal directions. This technique of scanning SAXS allows an accurate and reproducible determination of the beam position on the sample and an efficient collection of scattering patterns at positions of interest (Fratzl *et al.*, 1997).

In practice we obtained the information on the beam position by rapid scanning of the whole sample in steps of 200  $\mu\text{m}$  and recording the total intensity at each position (SAXS tomography). Since the total scattering intensity can be considered roughly proportional to the amount of scattering material irradiated by the beam, it can be used for determining the beam position on samples that are inhomogeneous in density. In the case of wood, the difference in density of early wood and late wood allows one to image the annual rings in a radial section. In a second step, several points of interest were chosen for small-angle X-ray scattering. Scattering patterns were recorded within typically 3 h in order to obtain good statistics. Extensive scans over radial slices were carried out, and the MFA was determined from the scattering pattern at each measurement point and correlated with the distance from the pith.

All samples were characterized by taking polarization-microscope images from cross sections cut from the same block as the sample used for SAXS.

### Data Evaluation

The intensity of the radiation scattered by the wood cell wall at small angles can be written as

$$I(\mathbf{q}) = I_0 (\rho_{\text{Cellulose}}^e - \rho_{\text{Matrix}}^e)^2 \left| \int_V \exp(i\mathbf{q}\mathbf{r}) d^3r \right|^2 \quad (1)$$

(Jakob *et al.*, 1995),

where  $\mathbf{q}$  is the wave vector of the scattered beam, related to the scattering angle  $2\theta$  between the incident and the scattered beam

by  $|\mathbf{q}| = (4\pi/\lambda) \sin \theta$ , and  $(\rho_{\text{Cellulose}}^e - \rho_{\text{Matrix}}^e)$  is the electron density contrast between the cellulose elementary fibrils and the surrounding matrix. This formula applies for cell walls hydrated above the fiber saturation point and  $|\mathbf{q}| > 0.3 \text{ nm}^{-1}$ , where a contribution from pore scattering can be excluded (Jakob *et al.*, 1996). The scattering vector  $\mathbf{q}$  can be expressed in polar coordinates  $(q, \chi)$  and  $I(\mathbf{q})$  as  $I(q, \chi)$ , where  $q$  is the length of  $\mathbf{q}$  and  $\chi$  the azimuthal angle of  $\mathbf{q}$  in the detector plane. The integral in Eq. (1) yields information on shape, size, and orientation of the cellulose fibrils. The fibril orientation and thus the microfibril angle can be extracted from the angular distribution of the scattered intensity

$$H(\chi) = \int_{q_1}^{q_2} I(q, \chi) dq. \quad (2)$$

The scattered intensity obtained from the experiment was therefore integrated over  $q$  and plotted versus the azimuthal angle  $\chi$ . The lower integration limit  $q_1$  (here:  $0.35 \text{ nm}^{-1}$ ) was chosen such that pinhole scattering and scattering from pores was excluded from the evaluation (Jakob *et al.*, 1996), the upper limit  $q_2$  (here:  $2.15 \text{ nm}^{-1}$ ) was determined by the size of the detector area. The resulting curve was then evaluated to obtain the microfibril angle quantitatively.  $H(\chi)$  in Eq. (2) does not depend only on the microfibril angle distribution but is a function also of the orientation distribution of the cell walls and thus of the cell shape. This is illustrated in Fig. 1, where  $\mu$  is the microfibril angle and  $\alpha$  denotes the orientation of a cell wall. The orientation  $\chi$  of the resulting streak on the detector is given by

$$\tan \chi = -\tan \mu \cdot \cos \alpha. \quad (3)$$

For the evaluation of cells with different shapes, i.e., different distributions of  $\alpha$ , different procedures must be applied. We closely followed the evaluation method described in detail in Lichtenegger *et al.* (1998). Here, only a short overview will be given:

*Cells with a rectangular cross section.* If the sample is positioned such that the beam hits the cell at right angles, the scattering pattern is a superposition of three streaks: one at  $\chi = 0$ , two at  $\chi = \pm \mu$ . Hence, at this sample position,  $\mu$  can be determined directly (Reiterer *et al.*, 1997; Lichtenegger *et al.*, 1998). In reality there is not only a single spiral angle  $\mu$  but a distribution of spiral angles  $f(\mu)$  about a mean value of  $\mu$ . In case of rectangular cells this leads to a broadening of the streaks, the intensity distribution in  $\chi$  being proportional to  $f(\mu)$ .

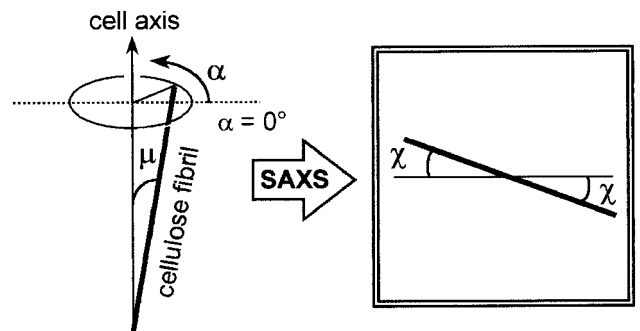


**FIG. 1.** The small-angle scattering from a cellulose fibril yields a narrow streak on the detector, whose orientation  $\chi$  was determined by the microfibril angle  $\mu$  versus the longitudinal cell axis and the rotation angle,  $\alpha$ , of the fibril around the cell axis.  $\alpha = 0^\circ$  denotes the plane of observation.

*Cells with a round cross section.* For cells with circular cross section and a microfibril angle distribution  $f(\mu)$ , the intensity distribution measured on the detector becomes

$$H(\chi) = 4 \int_{\chi}^{\pi/2} \frac{f(\mu) \sin(\mu)}{\sqrt{\cos^2 \chi - \cos^2 \mu}} d\mu \quad (4)$$

(Perret and Ruland, 1969). By inverting Eq. (4) one can in principle calculate the microfibril angle distribution  $f(\mu)$  exactly. Given the limited accuracy of the experimental determination of  $H(\chi)$ , we used a simpler approach described in Fratzl *et al.* (1996).

Here, the experimental data could always be fitted with a Gaussian distribution  $f(\mu)$ , in the case of rectangular cells as well as in the case of round cells, and the MFA distributions could therefore be compared directly.

## RESULTS

### *Picea abies* (Norwegian Spruce)

Figure 2 shows a polarized light microscopic image of a cross section taken from a stem of *P. abies*. The tracheids are typically regularly ordered and almost perfectly rectangular in cross section. The thin-walled cells with large lumen are early wood cells (EW), and the thick-walled ones belong to late wood (LW). In Fig. 3 typical scattering patterns and the evaluation with regard to the microfibril angle distribution are shown. The scattering pattern in Fig. 3a (1) is a superposition of three streaks, as expected for rectangular cells oriented perpendicular to the incident beam (see evaluation section). The longitudinal

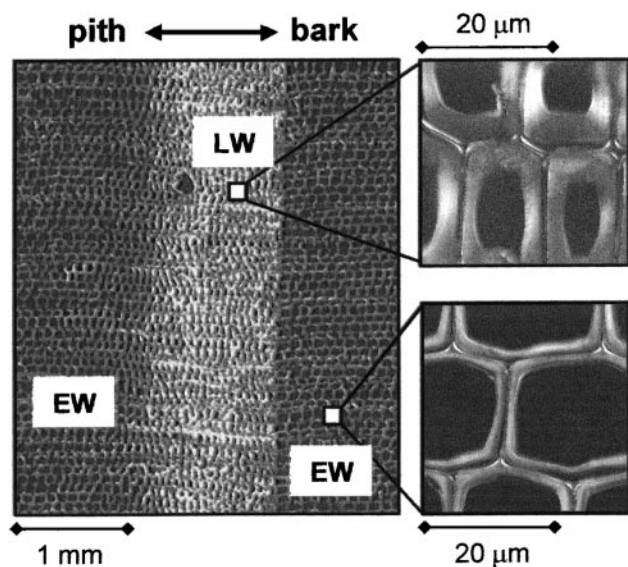


**FIG. 2.** Polarization microscopic image of a cross section of *Picea abies* (stem, mature wood). The direction of growth is from the left to the right, as denoted on the top of the figure. The right panel shows thick-walled late wood (LW) tracheids and thin-walled early wood (EW) tracheids in greater magnification. Note the rectangular shape and the regular order of the cells.

cell axis was oriented vertically. In Fig. 3a (2) the data integrated over  $q$  are plotted versus the azimuth  $\chi$ . The curve could be fitted with three Gaussians of equal width. Figure 3a (3) shows the resulting MFA distribution: a Gaussian centered at  $19.9^\circ$  and with a width of  $\sigma = 8^\circ$ . A mean MFA of  $20^\circ$  had been found to be typical for mature late wood in *P. abies* (Jakob *et al.*, 1994). The scattering pattern in Fig. 3b (1) was obtained from mature early wood and consisted of only one narrow streak. Integrating the data over  $q$  gave a narrow peak (Fig. 3b (2)). Assuming the same distribution width as in late wood ( $\sigma = 8^\circ$ ), one single Gaussian sufficed for a good fit. This corresponds to a mean microfibril angle of  $0^\circ$  and a distribution width of  $\sigma = 8^\circ$ , as had been found in early wood in a number of individuals of *P. abies* (Jakob *et al.*, 1994).

### *Pinus sylvestris* (Scots Pine)

In Fig. 4, a microscope image of a cross section of *P. sylvestris* (stem) is shown. *P. sylvestris* also belongs to the softwoods, but its tracheids are much less regular in cross section and order than those of *P. abies*. As in *P. abies*, EW and LW can be distinguished by the thickness of the cell wall and the size of the lumen. In Fig. 5a (1) a typical scattering pattern from juvenile wood near the pith is shown. The fit with three Gaussians (Fig. 5a (2)) yielded a mean microfibril angle of  $29^\circ$  and a distribution width of  $10.5^\circ$  (Fig. 5a (3)). Below, in Fig. 5b (1), the scattering pattern of mature late wood is shown. There is only a single broad streak without any visible splitting. Upon integration we obtained a broad peak that could be fitted either with three Gaussians (Fig. 5b (2)) or, equally well, with just a single broad Gaussian (Fig. 5b (4)). The two fits yield different MFA distributions: a mean MFA of  $15.7^\circ$  and a distribution width of  $8.6^\circ$  (Fig. 5b (3)) or a mean MFA of  $0^\circ$  and a distribution width of  $14.5^\circ$  (Fig. 5b (5)), respectively. In a SAXS measurement these two MFA distributions both yield the same experimental data and thus cannot be distinguished.

### *Quercus robur* (Pedunculate Oak)

Figure 6 shows a microscopic picture of a cross section of *Q. robur* (stem). Like all hardwoods, *Q. robur* consists of a variety of cell types: vessels for conducting water, libriform fibers and fiber tracheids for mechanical support, parenchyma cells for nutrient storage, etc. Since *Q. robur* is a ring porous hardwood species, the large early wood vessels are agglomerated in rings, allowing an easy distinction between EW and LW. Also the late wood cells are organized in groups: (a) the libriform fibers and (b)

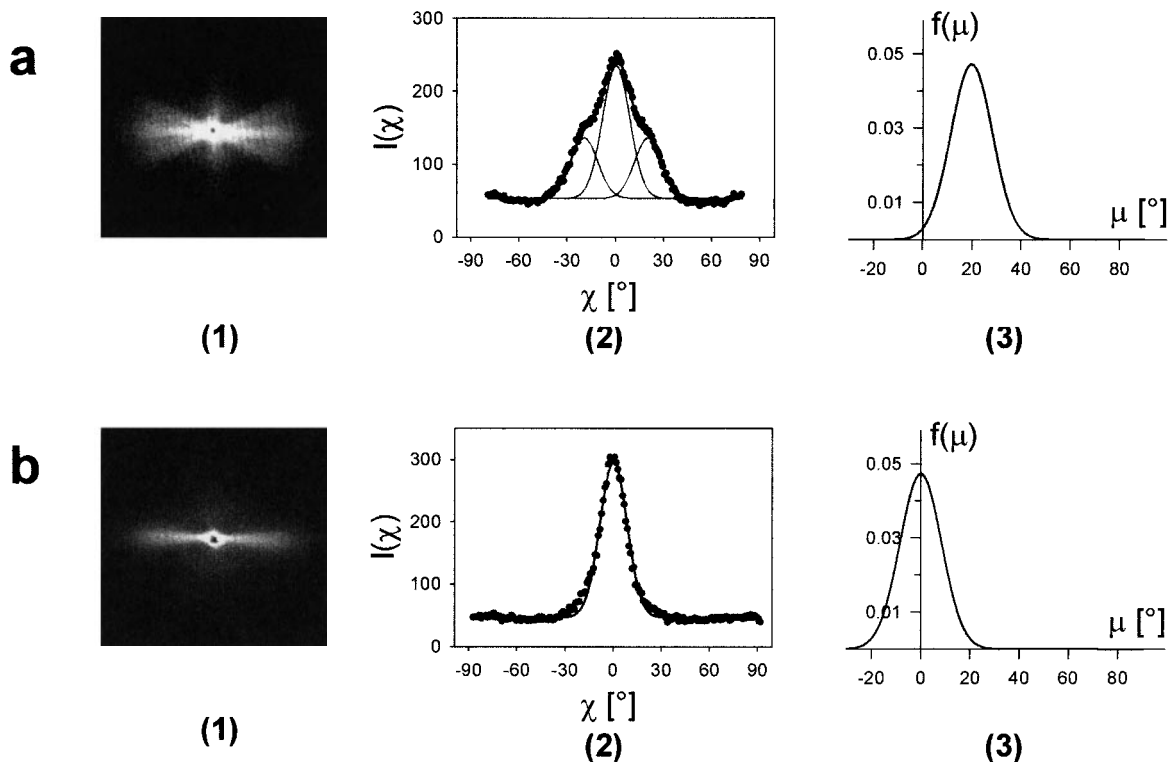


**FIG. 3.** (a) (1) Typical small-angle X-ray scattering pattern obtained from *P. abies* late wood. The longitudinal tracheid axis was vertical. The three streaks in the pattern correspond to the scattering expected from rectangular cells hit at right angles by the beam (scattering from the major cell wall layer, the S2 layer). The weaker vertical streak is due to scattering from the thin S1 layer. (2) The intensity of the scattered radiation was integrated over the scattering vector  $q$  and plotted versus the azimuth  $\chi$ . Since the scattering patterns from SAXS are symmetric by principle, only one half of the pattern needs to be evaluated. The curve could be fitted with three Gaussians. (3) The microfibril angle distribution  $f(\mu)$  was a Gaussian with mean value  $19.9^\circ$  and a Gaussian width of  $\sigma = 8^\circ$ . (b) (1) Scattering pattern obtained from *P. abies* early wood, consisting of only one narrow streak. (2) Integration of the data over  $q$  yielded a narrow peak that could be fitted with a single Gaussian. (3) The mean MFA was  $0^\circ$ , and the distribution width was  $\sigma = 8^\circ$ .

the latewood vessels and fiber tracheids, resulting in radial stripes.

With help of the scanning SAXS technique (Fratzl *et al.*, 1997), we succeeded in discriminating the two cell groups in a tangential section of *Q. robur* late wood and recording separate scattering patterns. Libriform fibers were recognized due to their thicker cell walls and smaller lumen (Fig. 6, right panel) yielding a higher total SAXS intensity. The cell groups were about 0.5 to 1 mm wide in tangential direction, so the position resolution of 200  $\mu\text{m}$ , given by the size of the beam, sufficed to image the alternation of libriform fiber regions with vessel regions. In Fig. 6, on the left edge, the total scattered intensity recorded at each point of a scan through a tangential slice is plotted versus the position on the sample. The dashed line through the central picture indicates where the scan was performed. Higher intensity indicates a predominance of libriform fibers, and lower intensity late wood vessels and fiber tracheids. This allowed the SAXS data to be assigned to the cell type.

In Figs. 7a (1) and 7b (1) scattering patterns obtained from libriform fibers are shown. Whereas 7a was recorded in the second annual ring, 7b was recorded in mature wood. Since the libriform fibers are round cells, the data were fitted according to the method described in Fratzl *et al.* (1997) (Figs. 7a (2) and 7b (2)). The mean MFA was  $23.3^\circ$  in the case of juvenile wood and  $0^\circ$  in the case of mature wood. The widths of the distributions were  $7.5^\circ$  and  $6.4^\circ$ , respectively. In Fig. 7c (1) a scattering pattern from late wood vessels and fiber tracheids is shown. The scattered intensity was low due to the thinner cell walls and the signal was broad (Fig. 7c (2)). This is, indeed, much different from the signal obtained from libriform fibers, although it was recorded in the same annual ring. The fit yielded a very broad MFA distribution centered at  $0^\circ$  and with a width of  $22^\circ$  (Fig. 7c (3)). Note that without experimental separation of libriform fibers from late wood vessels and fiber tracheids, one would always observe a superposition of these X-ray patterns. In practice, the signal from the late wood vessels and fiber tracheids would

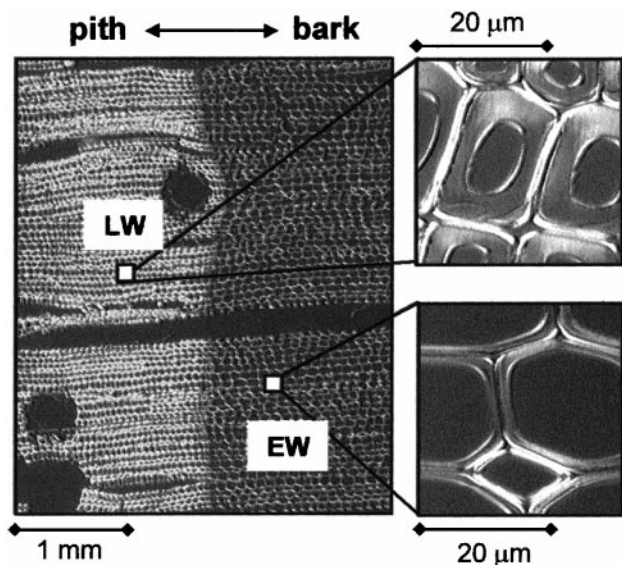


**FIG. 4.** Cross section of *Pinus sylvestris* (stem, mature wood) under the polarized light microscope. EW and LW can be distinguished by the thickness of the cell wall and the size of the lumen (see the greater magnification in the right panel). The cell shape is near to rectangular, but less regular than that in *P. abies*. The round holes seen in the picture in the left panel are resin canals.

probably be overlooked because of its comparative weakness. In Fig. 7d (1) the scattering from early wood tracheids is depicted. The integration over  $q$  clearly shows that there is no preferred orientation (Fig. 7d (2)).

#### *F. sylvatica* (Copper Beech)

In *F. sylvatica*, a diffuse porous hardwood species, early wood and late wood cannot be distinguished as easily as in ring porous hardwoods, because the transition from EW to LW is continuous and the distribution of vessels is random (Fig. 8). But still the density is higher and the vessels are smaller in late wood than in early wood. Since, in contrast to *Q. robur*, there are no particular agglomerations of cells, it was not possible to take separate SAXS patterns from different cell types, but the scattering signal was a superposition of contributions from all kinds of cells.

In Fig. 9 two typical scattering patterns are displayed. Figure 9a (1) shows a typical scattering pattern from juvenile wood. The peak obtained by integration over  $q$  was broad and the MFA distribution derived from the fit according to the fit for round cells (Fratzl *et al.*, 1996) was centered at  $0^\circ$ , with a width of  $13.9^\circ$  (Fig. 9a (3)). Figure 9b (1) shows the scattering pattern of mature wood. It consists of a strong single streak and a weak contribution of two inclined streaks. The contributions were fitted separately (Fig. 9b (2)), yielding an MFA distribution

(Fig. 9b (3)) that could be expressed as the sum of a narrow Gaussian centered at  $0^\circ$  and a broader Gaussian centered at  $30^\circ$ , normalized to their relative intensities in the scattering pattern. In analogy to *Q. robur*, one may assume that the strongest part of the signal was due to the scattering from the libriform fibers and the weaker signal indicating a larger MFA and a broader distribution should be assigned to vessels and libriform fibers.

#### Comparison

In Fig. 10 the plots of the MFA versus distance from the pith in all four wood species investigated are arranged side by side for comparison: (a) *P. abies*, (b) *P. sylvestris*, (c) *Q. robur*, and (d) *F. sylvatica*. It is obvious, with the exception of (d), that the microfibril angle decreased from pith to bark. There were, however, differences regarding the detailed course of microfibril angle with increasing stem diameter.

In *P. abies* (Fig. 10a) the microfibril angle decreased from about  $30^\circ$  near the pith to  $0^\circ$  near the bark. In the range of 50 to 130 mm from the pith the MFA values of early wood (open symbols) and late wood (filled symbols) stayed at constant but considerably different values:  $0^\circ$  in early wood and  $20^\circ$  in late wood. This behavior had been found in a number of individuals of *P. abies* (Jakob *et al.*, 1995; Reiterer *et al.*, 1998). In the outermost annual rings the MFA in late wood suddenly dropped to  $0^\circ$ , to the value found in early wood, and remained constant for the rest of the annual rings. In some annual rings nearer to the pith late wood a MFA of  $0^\circ$  was observed, too, but these results should be regarded with care. In those annual rings the proportion of late wood was so low that it was difficult to measure exclusively late wood and therefore the scattering patterns might as well contain scattering from early wood.

In *P. sylvestris* (Fig. 10b) the decrease of the MFA from the pith toward the bark was more gradual than that in *P. abies*. In contrast to *P. abies*, the MFAs in early wood were higher than those in late wood. The data were fitted with three Gaussians, except in a few cases where the fit with three Gaussians yielded unreasonable results, like a distribution width much higher than the mean fibril angle or a distribution width considerably smaller than  $7^\circ$ . In those cases the data were fitted with single Gaussians only, yielding a mean MFA of  $0^\circ$ . In any case, the width of the MFA distribution derived from the SAXS patterns (indicated by error bars) was larger than in that *P. abies*.

In Fig. 10c, results from *Q. robur* are shown. The microfibril angle decreased from  $20^\circ$  near the pith to  $0^\circ$  at a distance of about 40 mm from the pith and then stayed approximately constant. The full circles denote the contribution from libriform fibers. The

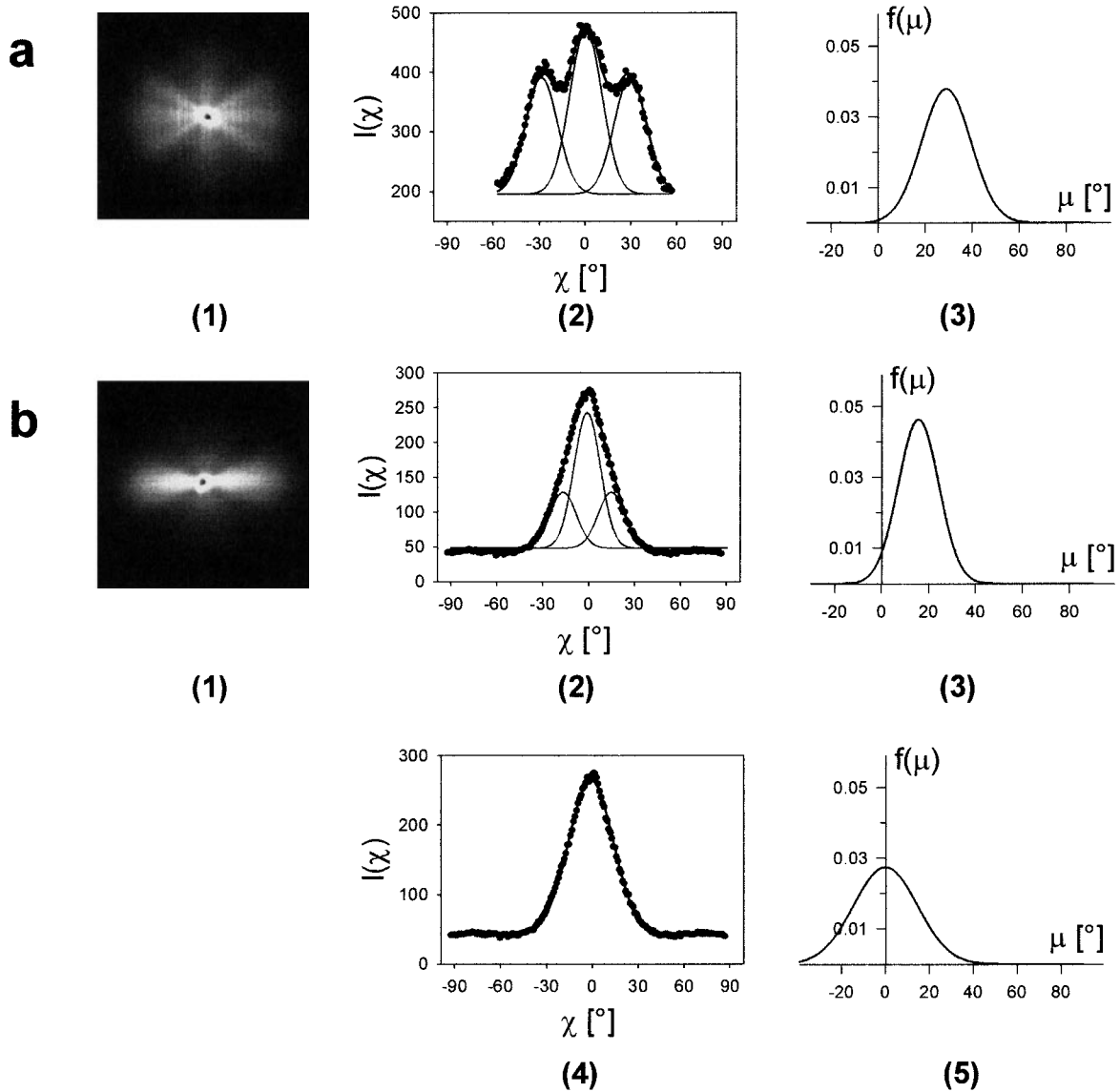


**FIG. 5.** (a) (1) Small-angle scattering pattern obtained from *P. sylvestris* juvenile wood in the second annual ring. The scattering pattern consisted of three clearly split streaks (S2 layer) and a weaker vertical streak that corresponds to scattering from the S1 layer. (2) Upon integration of the scattered radiation intensity over the scattering vector  $q$  we obtained three peaks that could be fitted with three Gaussians. (3) The mean MFA was  $29^\circ$ , and the width of the MFA distribution  $f(\mu)$  was  $10.5^\circ$ . (b) (1) Scattering pattern recorded in the 50th annual ring of a *P. sylvestris* stem (mature wood). There was only a single broad streak without any visible splitting. (2) After integration over  $q$ , the data could be fitted with three Gaussians. (3) The fit with three Gaussian peaks yielded an MFA distribution that peaked at  $15.7^\circ$  and whose width was  $8.6^\circ$ . (4) An alternative way of fitting with only one single Gaussian peak. The quality of the fit was equal to the one obtained with three Gaussians shown in (2). (5) The MFA distribution  $f(\mu)$  derived from the fit with a single Gaussian was centered at  $0^\circ$  and the width ( $\sigma = 14.5^\circ$ ) was considerably larger than that of the three-peak fit.

insert in Fig. 10c shows the microfibril angle in late wood vessels and fiber tracheids (small diamonds).

In *F. sylvatica* (Fig. 10d) the MFA calculated from the strongest component of the scattering signal assigned to libriform fibers was generally small, even near the pith, where it was still found to be  $0^\circ$ , only the distribution width was larger. The MFA stayed constant over the whole stem. The weak contribution of cell walls

with a microfibril angle of about  $30^\circ$ , probably vessels and fiber tracheids, is denoted by small diamonds.

## DISCUSSION

Although there are great differences in cell architecture among the four investigated wood species on the microscopic scale, in particular between soft-

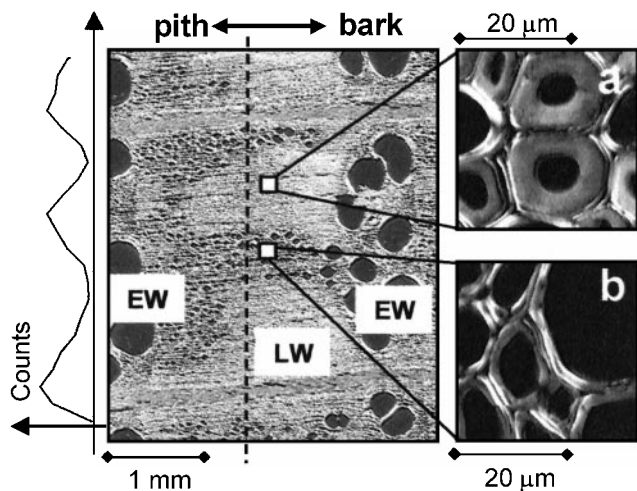


**FIG. 6.** Polarization microscopic image of a cross section of *Quercus robur* (stem, mature wood). *Q. robur* is a ring porous hardwood species, so called because of the characteristic arrangement of large EW vessels in concentric rings. In the LW, different cell types are arranged in groups that form irregular radial stripes: round, thick-walled libriform fibers with small lumen (shown in greater magnification in the right panel (a)) and thin-walled late wood vessels surrounded by fiber tracheids (right panel (b)). The cells arranged in straight horizontal lines, one at the top, one at the bottom of the picture in the left panel, are radially running parenchyma cells. Rapid scanning of the X-ray beam along the dashed line over a tangential slice prepared out of exclusively late wood yielded a variation of the total scattered intensity recorded at each point with the scan position, as displayed on the very left edge. A higher total intensity can be assigned to libriform fibers and a lower intensity to late wood vessels and fiber tracheids.

woods and hardwoods (see, for example, Grosser, 1977), we observed a consistent trend of the mean microfibril angle to decrease from pith to bark, with the exception of *F. sylvatica*, where only the MFA distribution was found to be higher near the pith. However, in softwoods the microfibril angles were significantly higher than those in the hardwood species, not only near the pith, where they reached up to 45° in contrast to 20° in *Q. robur* and even 0° in *F. sylvatica*, but stayed higher over a wider range of annual rings and dropped to very small values only in the outer part of the stem.

Comparing the two softwoods, the most striking difference is the fact that in *P. abies* the microfibril angle in early wood was lower (0°) than that in late wood (20°), whereas in *P. sylvestris* the opposite trend was found: the MFA was always about 5–10° higher in early wood than in late wood. It should be noted, however, that the MFA distribution width in *P. sylvestris* was relatively large (up to 13°) and therefore the determination of small fibril angles was not very accurate. Since the quantitative evaluation of microfibril angles is sensitive to the cell shape, the broadening of the streaks may be due to

the somewhat irregular shape of cells that can only be roughly approximated by rectangles (compare Fig. 4). On the contrary, in *P. abies* the Gaussian width of the MFA distribution was only 5–8°, allowing a more accurate determination of fibril angles. So the abrupt jumps of microfibril angles between two discrete values (0° and 20°) within each annual ring over a wide range of the stem are with certainty not due to artifacts and therefore particularly remarkable. The same abrupt alternation between 0° and 20° had been found in a number of individuals of *P. abies* (Jakob *et al.*, 1994, 1995; Reiterer *et al.*, 1999), but has not to our knowledge been observed in any other wood species.

In contrast to softwoods, hardwoods are generally quite difficult to investigate by X-ray scattering, due to their more complex anatomy. The major problem is the fact that various cell types are hit by the beam simultaneously. Their contribution to the scattering signal cannot be separated. Using the technique of scanning SAXS, we succeeded in overcoming the problem of signal superposition in the case of *Q. robur* and obtained separate information on the microfibril angle in different cell types in hardwood. Indeed, the microfibril angle distribution in the libriform fibers was different from that in vessels and fiber tracheids. However, by far the strongest contribution comes from the libriform fibers, whose thick cell walls represent the major part of cell wall material. Thus for an interpretation in terms of mechanical optimization of the whole composite, it may suffice to consider only the microfibril angle of libriform fibers. This should also apply to *F. sylvatica*. Regarding the libriform fibers, in both species small angles were found throughout the stem, except for the very first annual rings in *Q. robur*.

#### *Interpretation in Terms of Mechanical Optimization*

In this section we speculate that the general decrease of microfibril angles from pith to bark corresponds to a mechanical optimization process. In particular, we consider three different loading conditions of a stem or branch which is very roughly described by a cylinder of constant diameter  $D$  and height  $H$ . In Fig. 11 the three situations are sketched. All the estimates in this section are taken from the textbook by Landau and Lifschitz (1986); some of the equations can also be found in Ashby (1983) and Mattheck and Kubler (1995).

(a) *Lateral forces (e.g., wind)*. Given a lateral force  $F_L$ , the largest bending moment of a stem will be

$$M = F_L H = \frac{EI}{R}, \quad (1)$$

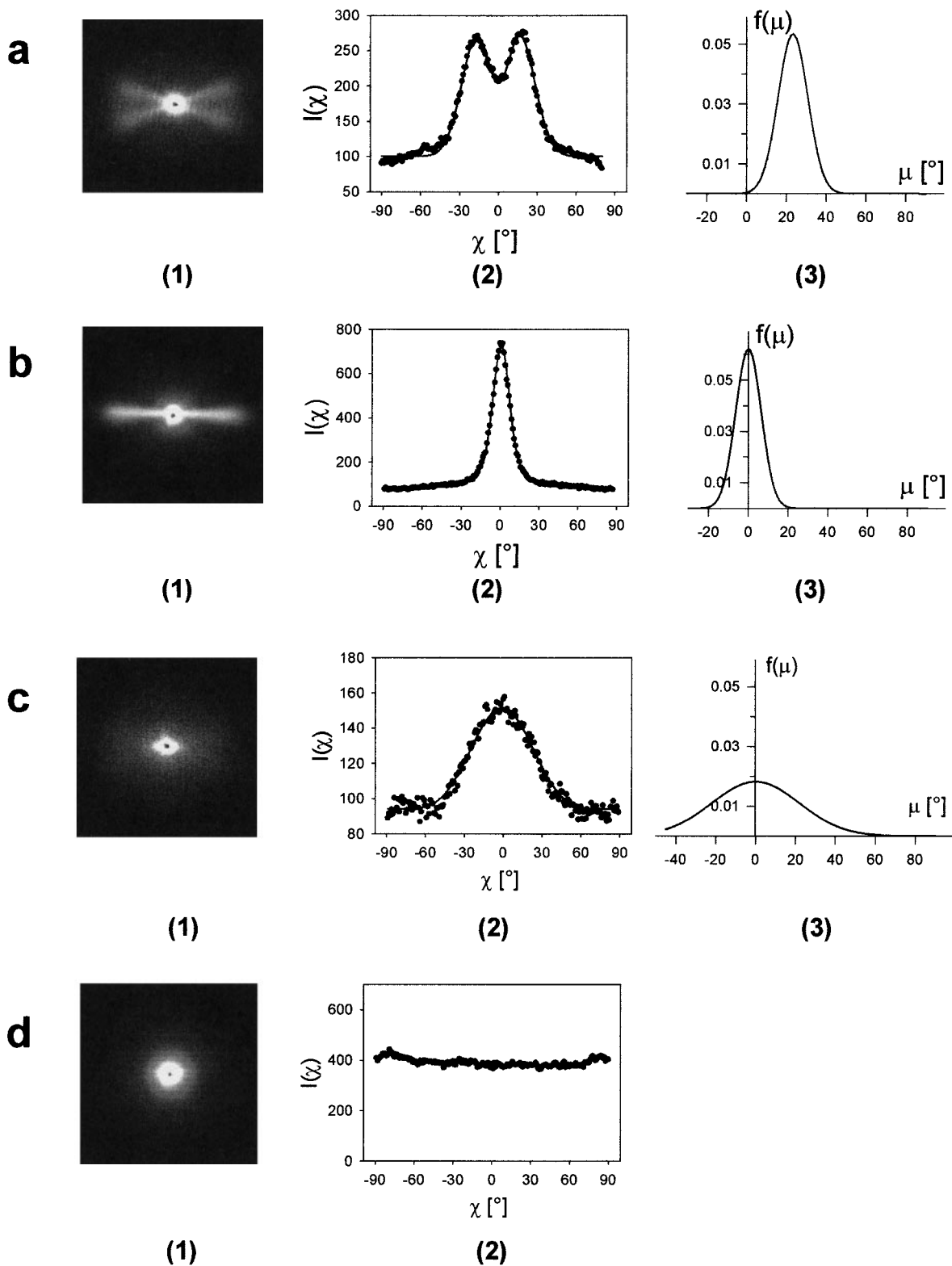


**FIG. 7.** (a) (1) Small-angle X-ray scattering obtained from libriform fibers in the second annual ring of a stem of *Q. robur*: One can clearly see the splitting of the scattering pattern into two streaks. (2) The data were integrated over  $q$ , plotted versus the azimuth  $\chi$ , and fitted according to the method described in this paper for round cells. (3) MFA distribution calculated from the fit: a Gaussian centered at  $23.3^\circ$  with a width of  $\sigma = 7.5^\circ$ . (b) (1) Small-angle scattering from mature libriform fibers in *Q. robur*: the scattering pattern consisted only of a narrow streak. (2) Integration over  $q$  yielded a narrow peak that was again fitted with the method used for round cells. (3) The MFA

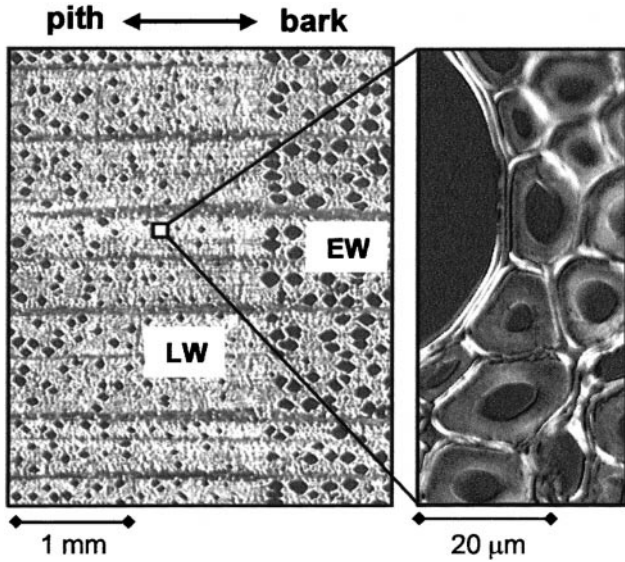


**FIG. 8.** Cross section of *Fagus sylvatica* (stem, mature wood) under the polarization microscope. *F. sylvatica* is a diffuse porous hardwood, i.e., the vessels are distributed randomly in early wood and late wood. In EW the size of the vessels is larger than that in LW and thus the density is lower. The right panel shows a vessel surrounded by thick-walled libriform fibers in greater magnification.

where  $E$  is the Young's modulus,  $I$  is the moment of inertia, and  $R$  is the radius of curvature of the stem. The stresses occurring on the surface of the cylinder (tensile ones on the side where  $F_L$  is applied, compressive ones on the opposite side) are given by  $\sigma = (D/2) E/R$ . Let  $\sigma_0$  be the maximum stress that can be supported by the material. For a given diameter of the trunk  $D$  and for given lateral forces  $F_L$ , the height of the trunk is limited to

$$H < \frac{2 I}{D F_L} \sigma_0, \quad (2)$$

where  $I$  can also be replaced by  $\pi D^4/64$  for a trunk with a circular cross section. This means that the height is effectively limited by  $\sigma_0$ .

(b) *Vertical compressive forces due to gravitation.* In this situation, the height is limited by the buckling instability of the cylinder, which yields

$$H < \frac{\pi}{2} \sqrt{\frac{E I}{F_G}}, \quad (3)$$

where  $F_G$  is the gravitational force. The limiting factor for the height is the elastic modulus, which means that the material should be optimized for maximum stiffness.

(c) *Bending up to a critical angle.* This point is based on the idea that in order to avoid breaking due to a moving obstacle, such as, e.g., a large animal, passing by, the tree has to bend up to a critical angle  $\theta_0$ . Similarly, considering a branch,  $\theta_0$  could be the critical angle where, for example, snow glides off. Bending up to an angle  $\theta_0$  results in a bending moment  $M = F_0 x$ ,

$$\text{where } x = \sqrt{\frac{2 I E}{F_0} \cos \theta_0}.$$

The force  $F_0$  is the largest force before the branch or trunk is relieved by either the snow gliding off or the animal passing over.  $F_0$  and  $\theta_0$  are related by

$$H = \sqrt{\frac{I E}{2 F_0}} \int_{\theta_0}^{\pi/2} \frac{d\theta}{\sqrt{\cos \theta_0 - \cos \theta}}. \quad (4)$$

The largest bending moment that needs to be supported then becomes

$$M_0 = \lambda_0 I E/H, \quad (5)$$

where  $\lambda_0 = \sqrt{\cos \theta} \int_{\theta_0}^{\pi/2} d\theta / \sqrt{\cos \theta_0 - \cos \theta}$  is just a numerical factor depending on  $\theta_0$ . Consequently, the radius of curvature  $R$  due to the maximum bending moment  $M_0$  is

$$R = E I/M_0 = H/\lambda_0.$$

Finally, considering the fact that the largest strains occurring at the surface of the cylinder are given by  $\pm(D/2)/R$ , we get

$$H > \lambda_0 \frac{D}{2 \epsilon_0}, \quad (6)$$

where  $\epsilon_0$  is the largest strain that can be sustained by the material. Quite remarkably, condition (6) is a

distribution  $f(\mu)$  peaked at  $0^\circ$ , with a Gaussian width of  $\sigma = 6.4^\circ$ . (c) (1) Scattering pattern obtained from late wood vessels and fiber tracheids surrounding the late wood vessels in *Q. robur*: a single, very broad streak and a comparably weak signal (the data were collected in the same annual ring and within the same time as those in (b)). (2) The data were integrated over  $q$  and the fit method for round cells was applied. (3) The calculated MFA distribution was extremely broad ( $\sigma = 22.3^\circ$ ) and peaked at  $0^\circ$ . (d) (1) Small-angle scattering from *Q. robur* early wood (mainly large early wood vessels). (2) The integration of the scattered intensity over  $q$  revealed a random orientation of the cellulose fibrils in *Q. robur* early wood.

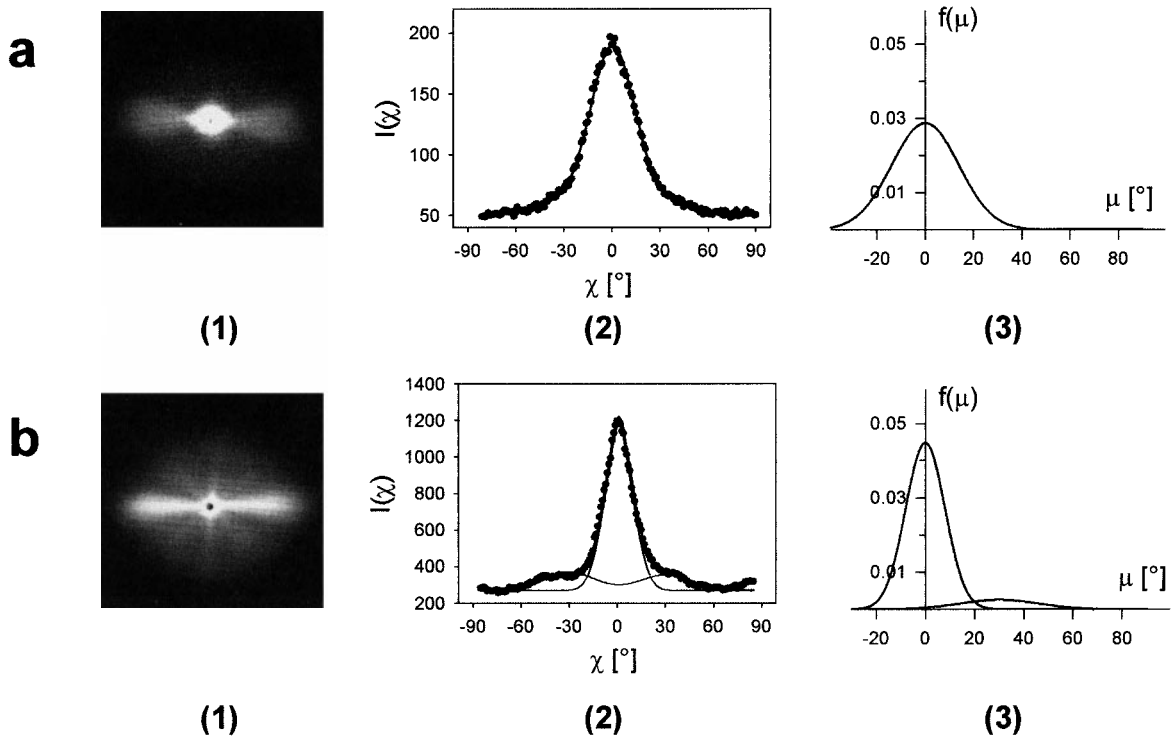


**FIG. 9.** (a) (1) X-ray scattering pattern recorded in juvenile wood (fifth annual ring) of a *F. sylvatica* stem. Only a single broad streak was observed. (2) Upon integration a broad peak was obtained and fitted according to the fit method for round cells. (3) The MFA distribution peaked at  $0^\circ$  and the Gaussian width was  $13.9^\circ$ . (b) (1) Scattering from *F. sylvatica* mature wood (80th annual ring). The pattern was a superposition of a strong, narrow streak and two weak, inclined streaks. (2) The curve resulting from the integration over  $q$  clearly showed the two contributions to the pattern. The narrow peak in the center and the split contribution were fitted separately, both assuming round cells. (3) The MFA distribution was given by the sum of a narrow distribution ( $\sigma = 8^\circ$ ) peaked at  $0^\circ$  and a broad distribution ( $\sigma = 16^\circ$ ) peaked at  $30^\circ$ . The two components were normalized to the intensities with which they appear in the scattering pattern.

lower bound for the height of the trunk (or the length of the branch). It also means that the lower the maximum strain,  $\epsilon_0$ , the larger the ratio  $H/D$  must be.

The analysis shows three ways of optimization in response to different loading situations: high fracture stress for resisting lateral forces, high elastic modulus for resisting compressive forces, or large fracture strain to survive bending. It is interesting to note that all three parameters have been shown to depend on the microfibril angle (Reiterer *et al.*, 1998; Cave and Walker, 1994). The trunk of a large tree will hardly be subjected to bending by animals passing by, but rather has to support lateral wind forces and compressive forces due to gravitation. Hence it seems reasonable to expect an optimization on the largest possible values for  $\sigma_0$  and  $E$ . This is, indeed, consistent with the fact that the MFA in the outer annual rings of a large tree was found to be close to  $0^\circ$ . For younger trees and branches, however, the loading situation (c) may become crucial and conditions (3) and (6) must be fulfilled simulta-

neously, that is

$$\lambda_0 \frac{D}{2 \epsilon_0} < H < \frac{\pi}{2} \sqrt{\frac{EI}{F_G}},$$

which implies that

$$E \epsilon_0^2 > \frac{64 \lambda_0^2 F_G}{\pi^3 D^2}.$$

It is obvious that the larger  $F_G$  and the smaller the diameter  $D$  of the trunk (this would correspond to a slim tree with a large height to diameter ratio and/or a comparatively large crown) the more stringent this condition becomes. It may well be that this is the reason the tree has to increase  $E \epsilon_0^2$  in its first years of life by an increased MFA. Indeed, our data for Norwegian spruce indicate an increase of  $E \cdot \epsilon_0^2$  with increasing microfibril angle from  $0^\circ$  to an angle of  $26^\circ$  by almost a factor of 5 (Fig. 12). This may explain the

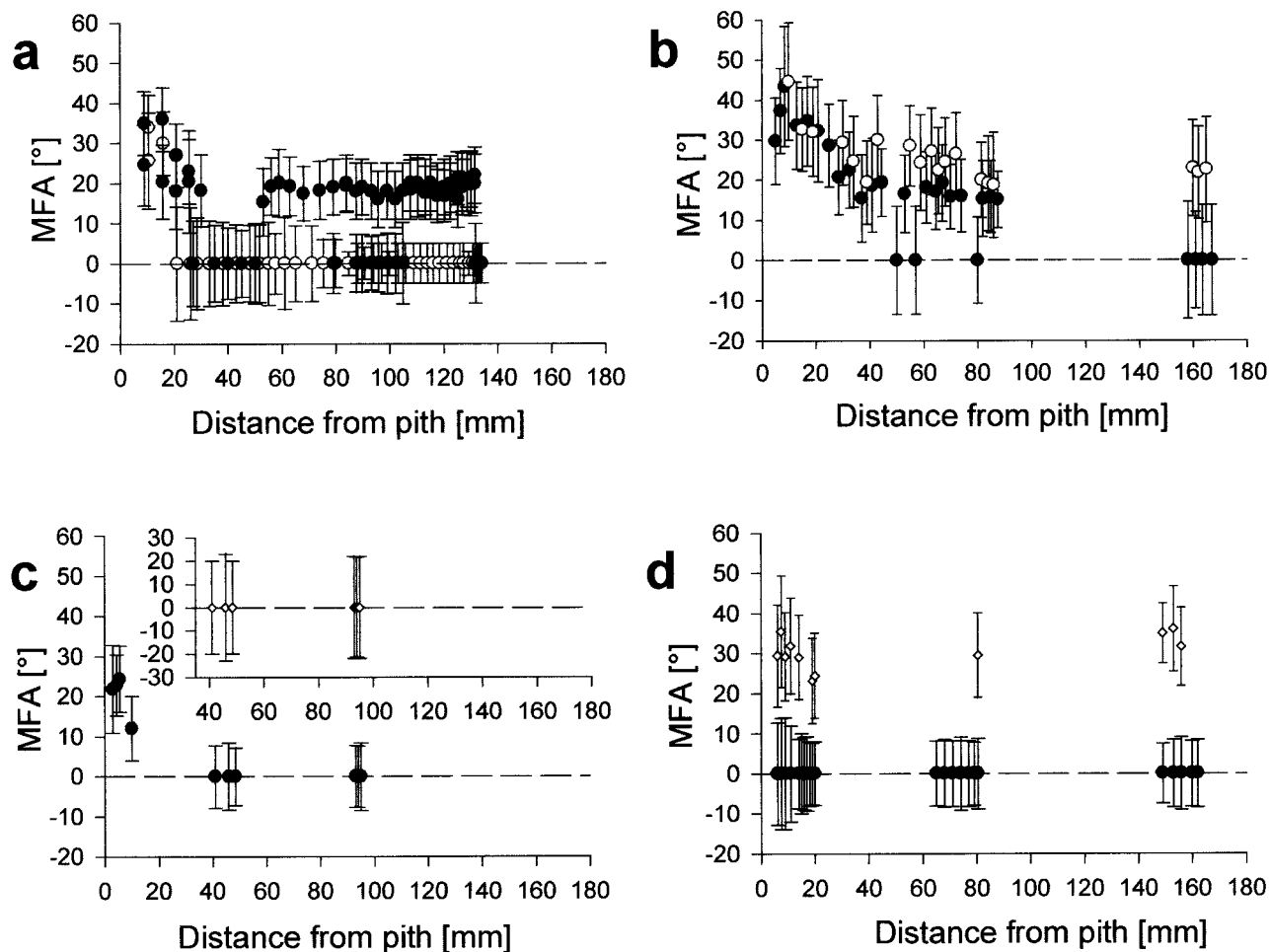


**FIG. 10.** Comparison of microfibril angles as a function of the distance from the pith. Full circles denote late wood, and open circles denote early wood. The error bars indicate the Gaussian width of the microfibril angle distribution. (a) *P. abies*: the microfibril angle decreased from 35° near the pith to 0° near the bark. In the region from 50 to 130 mm from the pith, the MFA was found to jump between two discrete values (0° in early wood and 20° in late wood) in each annual ring. In the outermost part of the stem the MFA in late wood dropped to 0°. Late wood with an MFA of 0° was also found in some annual rings nearer to the pith, but exclusively in those where the proportion of early wood was very low. (b) *P. sylvestris*: the MFA decreased from a maximum of 45° near the pith to smaller angles near the bark, in late wood even down to 0° in the last annual rings. In contrast to *P. abies*, the MFA in early wood was higher than that in late wood. (c) *Q. robur*: the plot consists of two parts: the main part containing full circles that denote the MFA measured in libriform fibers and a smaller plot at the top displaying the MFA as it was found in late wood vessels and fiber tracheids (small diamonds). For libriform fibers, maximum microfibril angles of about 20° were found near the pith. With increasing distance from the pith the MFA gradually decreased to 0° at 40 mm and stayed there in the rest of the stem. The MFA in late wood vessels and fiber tracheids (smaller plot) was about 0°, but the distribution width (denoted by the error bars) around the mean value was extremely broad. (d) *F. sylvatica*: the MFA in libriform fibers (denoted by full circles) was small throughout the stem radius, even close to the pith, where only a larger distribution around the mean MFA of 0° was observed. The small diamonds at MFA values of about 30° correspond to the microfibril angle determined from the weak part of the scattering signal that was assigned to late wood vessels and fiber tracheids.

frequent occurrence of microfibril angles about 30° near the pith. For larger MFAs as they are found on the lower side of conifer branches, the values of  $E \cdot \epsilon_0^2$  are even higher.

### CONCLUSION

In this paper we used position-resolved small-angle X-ray scattering to investigate the microfibril angles in two softwood species, *P. abies* and *P.*

*sylvestris*, and two hardwood species, *Q. robur* and *F. sylvatica*. As main results we found that: (1) Position-resolved SAXS is an appropriate tool in investigating anatomically complex hardwoods. It is possible to obtain separate information on the structures of different cells, at least in *Q. robur* or anatomically similar species. (2) Despite considerable differences in the detailed course of the microfibril angle with the annual rings, the MFA decreased from the pith to

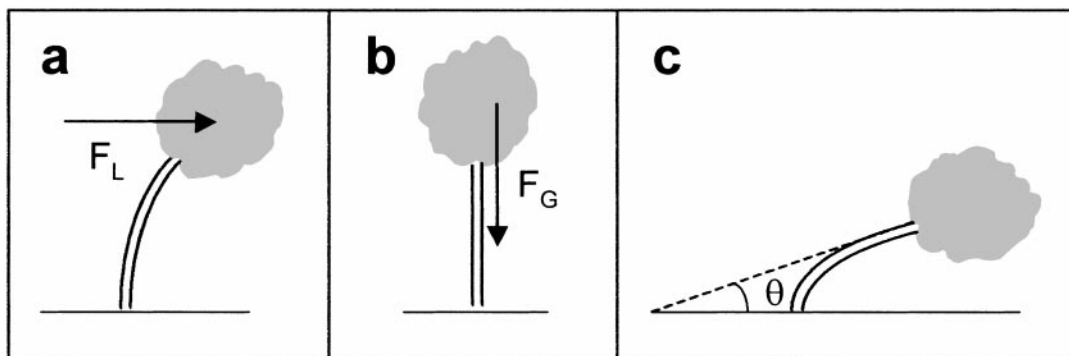


**FIG. 11.** Sketch of the three main loading conditions: (a) lateral wind forces, (b) gravitational forces, and (c) bending to a critical angle, for example, by animals passing by or until the snow glides off a branch.

the bark in all four trees. (3) The microfibril angles in the two hardwood species were generally lower than those in the two softwood species.

We suggest an interpretation of these results in terms of a mechanical optimization by different microfibril angles. Our model is based on the mechanical constraints to tree growth resulting from three main loading conditions of a tree: (a) lateral forces, (b) gravitational forces, and (c) bending to a critical angle. The last condition implies a maximization of  $E \cdot \epsilon_0^2$ , where  $E$  is the longitudinal Young's modulus and  $\epsilon_0$  is the fracture strain. As a consequence, loading condition (c) needs large MFAs, while both (a) and (b) require small MFAs. The typical decrease of microfibril angles from juvenile to mature wood would therefore result from different typical loading patterns during the development of the tree.

We thank G. Dinst from the Ludwig Boltzmann Institute for Osteology, Vienna, for the preparation of the cross sections for

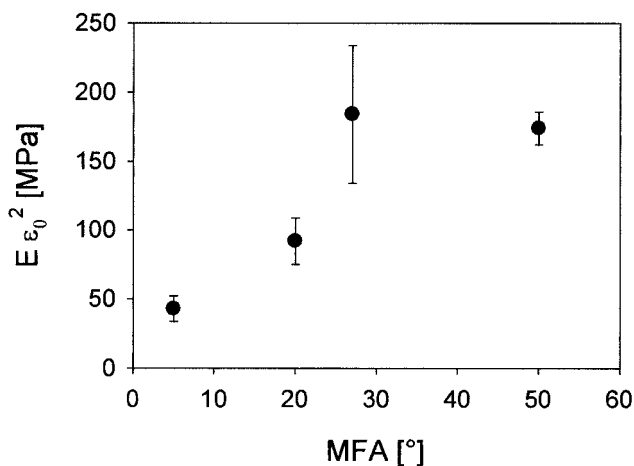


**FIG. 12.**  $E \cdot \epsilon_0^2$  ( $E$ , longitudinal Young's modulus;  $\epsilon_0$ , strain at maximum stress) plotted versus the microfibril angle. Data from Reiterer *et al.* (1999).

microscopy. We are grateful to the Fonds zur Förderung der Wissenschaftlichen Forschung (FWF) for financial support (Project P 10729-BIO).

## REFERENCES

- Ashby, M. F. (1983) The mechanical properties of cellular solids, *Met. Trans. A* **14**, 1755–1769.
- Cave, I. D. (1996) The longitudinal Young's modulus of *Pinus radiata*, *Wood Sci. Technol.* **1**(3), 268–278.
- Cave, I. D., and Walker, J. C. F. (1994) Stiffness of wood in fast-grown plantation softwoods, *Forest Products J.* **44**(5), 43–48.
- Fengel, D., and Wegener, G. (1984) *Wood Chemistry, Ultrastructure, Reaction*, De Grueter, Berlin.
- Fratzl, P., Paris, O., Klaushofer, K., and Landis, W. J. (1996) Bone mineralization in an Osteogenesis Imperfecta mouse model studied by small-angle X-ray scattering, *J. Clin. Invest.* **97**(2), 396–402.
- Fratzl, P., Jakob, H. F., Rinnerthaler, S., Roschger, P., and Klaushofer, K. (1997) Position resolved small-angle X-ray scattering of complex biological materials, *J. Appl. Crystallogr.* **30**, 765–769.
- Grosser, D. (1977) *Die Hölzer Mitteleuropas—Ein Mikrophotographischer Lehratlas*, Springer-Verlag, Berlin.
- Jakob, H. F., Tschegg, S. E., and Fratzl, P. (1994) Size and arrangement of elementary cellulose fibrils in wood cells: A small angle X-ray scattering study of *Picea abies*, *J. Struct. Biol.* **113**, 13–22.
- Jakob, H. F., Fengel, D., Tschegg, S. E., and Fratzl, P. (1995) The elementary cellulose fibril in *Picea abies*: Comparison of transmission electron microscopy, small-angle X-ray, and wide-angle X-ray scattering results, *Macromolecules* **26**, 8782–8787.
- Jakob, H. F., Tschegg, S. E., and Fratzl, P. (1996) Hydration dependence of the wood-cell wall structure in *Picea abies*. A small-angle X-ray scattering study, *Macromolecules* **29**(26), 8435–8440.
- Landau, L. D., and Lifschitz, E. M. (1986) *Theory of Elasticity (Course of Theoretical Physics, 7)*, Pergmon, Oxford.
- Lichtenegger, H., Reiterer, A., Stanzl-Tschegg, S. E., and Fratzl, P. (1998) Determination of spiral angles of elementary cellulose fibrils in the wood cell wall: Comparison of small-angle X-ray scattering and wide-angle X-ray diffraction, in Butterfield, B. G. (Ed.), *Microfibril Angle in Wood*, Proc. of the International Workshop on the Significance of Microfibril Angle to Wood Quality, New Zealand.

- Matthek, C., and Kubler, H. (1995) Timell, T. E. (Ed.), Wood—The Internal Optimization of Trees, Springer Series in Wood Science.
- Meylan, B. A. (1967) Measurement of microfibril angle in *Pinus radiata* by X-ray diffraction, *Forest Products J.* **15**(5), 51–58.
- Perret, R., and Ruland, W. (1969) Single and multiple X-ray small-angle scattering of carbon fibres, *J. Appl. Crystallogr.* **2**, 209–218.
- Preston, R. D. (1934) The organization of the conifer tracheid, *Philos. Trans. R. Soc. London Ser. B* **224**, 131–172.
- Preston, R. D. (1946) The fine structure of the wall of the conifer tracheid. I. The X-ray diagram of conifer wood, *Proc. R. Soc. London B* **133**, 327–347.
- Reiterer, A., Jakob, H. F., Stanzl-Tschegg, S. E., and Fratzl, P. (1998) Spiral angle of elementary cellulose fibrils in cell walls of *Picea abies* determined by small-angle X-ray scattering, *Wood Sci. Technol.* **43**(5), 335–345.
- Reiterer, A., Lichtenegger, H., Tschegg, S. E., and Fratzl, P. (1999) Experimental evidence for a mechanical function of the cellulose spiral angle in wood cell walls, *Philos. Mag. A.* **79**, 2173–2186.
- Sahlberg, U., Salmen, L., and Oscarsson, A. (1997) The fibrillar orientation in the S2-layer of wood fibres as determined by X-ray diffraction analysis, *Wood Sci. Technol.* **31**, 77–85.
- Wardrop, A. B. (1952) The low-angle scattering of X-rays by conifer tracheids, *Textile Res. J.* **22**, 288–291.